POLITECNICO DI TORINO
Repository ISTITUZIONALE

Cross-feeding percolation phase transitions of intercellular metabolic networks

Original
Cross-feeding percolation phase transitions of intercellular metabolic networks / Latoski, L.C.F., De Martino, A., De Martino, D.. - In: SCIENCE ADVANCES. - ISSN 2375-2548. - 11:36(2025). [10.1126/sciadv.adv8216]

Availability:
This version is available at: 11583/3003811 since: 2025-10-09T07:52:22Z

Publisher:
American Association for the Advancement of Science

Published
DOI:10.1126/sciadv.adv8216

Terms of use:

This article is made available under terms and conditions as specified in the corresponding bibliographic description in the repository

Publisher copyright

(Article begins on next page)

29 November 2026

Check for updates

NETWORK SCIENCE

Cross-feeding percolation phase transitions of intercellular metabolic networks

Luís C. F. Latoski[1]*, Andrea De Martino[2,3]*, Daniele De Martino[4,5]*

Copyright © 2025 The Authors, some rights reserved; exclusive licensee American Association for the Advancement of Science. No claim to original U.S. Government Works. Distributed under a Creative Commons Attribution NonCommercial License 4.0 (CC BY-NC).

Intercellular cross-talk is essential for the adaptation capabilities of populations of cells. While direct diffusion-driven cell-to-cell exchanges are difficult to map, current nanotechnology enables one to probe single-cell exchanges with the medium. We introduce a mathematical method to reconstruct the dynamic unfolding of intercellular exchange networks from these data, applying it to an experimental coculture system. The exchange network, initially dense, progressively fragments into small disconnected clusters. To explain these dynamics, we develop a maximum-entropy multicellular metabolic model with diffusion-driven exchanges. The model predicts a transition from a dense network to a sparse one as nutrient consumption shifts. We characterize this crossover both numerically, revealing a power-law decay in the cluster-size distribution, and analytically, by connecting to percolation theory. Comparison with data suggests that populations evolve toward the sparse phase by remaining near the crossover. These findings offer insights into the collective organization driving the adaptive dynamics of cell populations.

INTRODUCTION

The molecular revolution of the last century led to multiple breakthroughs in biology, culminating with the advent of whole-genome sequencing and its promises for personalized medicine. However, it also encountered a challenge: Is it possible to reconstruct complex physiological behavior from highly heterogeneous molecular interactions (*1*)? In response to this challenge, the "systemic" approach of systems biology shifted the focus from the nodes (molecules) to their interactions (*2*–*4*). While shedding light on many previously unseen aspects of biological systems, these methods often result in ad hoc models overloaded with molecular details, capable of reproducing empirical data but with limited generalization potential. By contrast, statistical mechanics has successfully explained macroscopic behavior by connecting molecular interactions and large-scale phenomena through highly generalizable frames in somewhat simpler physical systems, such as gases, magnets or metals (*5*), but also on more complex ones like glasses (*6*) or the brain (*7*), finding broad applicability in biophysics as well (*8*). At least in principle, the conceptual toolbox of statistical mechanics might hence be suited to yield fresh outlooks on systems biology as well.

Compared to physics, one of the major additional difficulties posed by living systems lies in the fact that they operate across a hierarchy of scales, from single molecules to ecosystems, with the cellular level arguably playing the central role. There is therefore a pressing need for research that addresses emergent phenomena across multi-scale interaction structures, particularly at the boundary between the molecular and cellular levels. In this article, we address one such structure, arising in the context of overflow metabolism.

The term "overflow metabolism" refers to the phenomenon whereby cells, despite having sufficient oxygen to fully oxidize incoming carbon (e.g., glucose), prefer to release partially oxidized compounds like lactate or acetate in the surrounding environment, thus renouncing potentially useful sources of energy. Such a behavior is ubiquitous in the cellular world (from bacteria to cancer cells) and is typically observed when cells are rapidly proliferating, in which case it is usually ascribed to nutrient uptake that exceeds the capacity of oxidative metabolism (respiration). In essence, in these conditions, cells appear to implement a cost-efficiency compromise by prioritizing less efficient, faster, but more wasteful metabolic pathways (like fermentation in yeast or aerobic glycolysis in cancer cells) over more efficient, slower, but less wasteful ones (*9*). Overflow metabolism in bacteria can indeed be well understood in terms of cell-autonomous trade-offs in the allocation of cellular resources (*10*–*13*). The case of mammalian cells—most notably, cancer cells—is however less clear (*14*–*17*). The main difference with microbial systems concerns the role of intercellular interactions (*18*). At odds with the cell-autonomous scenario, lactate accumulation in cancer cell cultures (also known as Warburg effect, the key signature of overflow metabolism in cancer) could indeed result from (a breakdown of) the collective organization of intercellular exchanges (*18*–*20*).

Cells adapting to an environment exchange chemical compounds for reasons ranging from signaling to cross-feeding. Exchanged compounds are usually by-products of the cells' metabolic activity that are excreted in the medium by one cell and are imported by another cell upon being sensed by specialized surface receptors. Uptake, in turn, affects the importer's metabolic activity, leading to a modulation of its secretions, i.e., to a new batch of signals that propagate across the population and trigger uptakes by other cells. As exchanges and interactions build up, they effectively establish a degree of decentralized cross-cellular coordination that facilitates the overall adaptation of the population to the medium and enables the engineering of a viable (shared) environment.

It is now known that overflow induces cell-to-cell interactions driven by exchanges of lactate (*19*). By balancing lactate excretion and import rates, populations can, in principle, control environmental lactate levels even in the presence of cells with sustained excretion rates. By contrast, a failure in this process can lead to the environmental lactate accumulation, i.e., to the Warburg phenomenon. The structure and dynamics of exchange networks therefore

[1]Instituto de Física, Universidade Federal do Rio Grande do Sul, CEP 91501-970 Porto Alegre, RS, Brazil. [2]Politecnico di Torino, Corso Duca degli Abruzzi 24, 10129 Torino, Italy. [3]Italian Institute for Genomic Medicine, SP142 Km 3,95, 10060 Candiolo, Italy. [4]Biofisika Institutua (UPV/EHU, CSIC) and Fundacion Biofisica Bizkaia, Leioa E-48940, Spain. [5]Ikerbasque Foundation, Bilbao, Spain.
*Corresponding author. Email: luis.latoski@ufrgs.br (L.C.F.L.); andrea.demartino@polito.it (A.D.M.); daniele.demartino@ehu.eus (D.D.M.)

Downloaded from https://www.science.org at Politecnico Di Torino on September 03, 2025

potentially encode a much more resolved picture of how a population of cells adjusts to and shapes its surrounding environment than the one provided, for instance, by macroscopic quantities such as the lag (adaptation) times in traditional growth curves.

Up to recent times, not much was known about these networks, although some of their properties were easy to guess. From a physics viewpoint, in fact, when cells have no mechanical contact with each other and no advective transport is present in the medium, the emergent interaction network is sustained by the diffusive motion of molecules. This implies that interaction networks are bound to be intrinsically stochastic, potentially lossy (due to signals being "perishable," in that the interaction-carrying molecule, once injected by a cell into the environment, could leave the system without being absorbed by another cell), dynamic (i.e., time dependent), and highly heterogeneous (as exchanges between distant cells are far less likely than exchanges between nearby cells). Advection, on the other hand, should give exchanges a preferential direction while simultaneously interfering with them, the latter tendency likely being dominant when the advection flow is more intense.

Recent developments in nanoscale technology applied to cellular systems in vitro, however, have lastly shed some light on these networks. In particular, techniques ranging from nanoscale mass spectrometry (*21*) to environment sensing through fluorescent nanofibers (*19*) now allow for direct or indirect quantification of single-cell exchange fluxes with the medium (i.e., the rates at which cells excrete or import certain compounds), even at high spatial and temporal resolutions. These types of data open a pathway to infer the time-varying structure of intercellular exchange networks.

Here, we study, both at the theoretical level and in data, the time evolution of the intercellular lactate exchange network in a specific empirical coculture system in which exchanges are driven by diffusion. In short, we will show that, as adaptation progresses, the exchange network evolves from a highly interconnected web to a sparse state characterized by multiple disconnected clusters of cross-feeding cells. By a theoretical analysis, we will then connect these results to the underlying metabolic activity of cells, showing that the emergence of the exchange network bears several hallmarks of a collective phenomenon, namely, a percolation-like transition. When projected onto the theoretical phase diagram, the empirical population appears to evolve in time toward a sparse phase by staying close to the transition region, through the gradual dilution of the initially dense exchange matrix.

The article is organized as follows. We first introduce a method to efficiently reconstruct diffusion-driven intercellular exchange networks from single-cell flux data. Empirical networks are then obtained by applying this protocol to the system studied in (*19*), revealing a crossover in time from a dense to a sparse state during adaptation. Next, this scenario is reproduced using a two-parameter maximum-entropy constraint-based computational model of the metabolic activity of cells which explicitly accounts for the possibility of lactate exchanges. This allows us to directly link the statistical features of the emergent exchange network to the metabolic decisions of individual cells. We then show that the dense-to-sparse crossover found in data can be described in terms of a percolation phase transition with a well-defined critical behavior that matches the empirical picture. Biological implications of these results are put forward in the last part of the article. Last, the generalization that includes an advective flow in the theoretical analysis is presented and discussed, along with details of the study, in the Supplementary Materials.

RESULTS

Network reconstruction problem

The experiments we consider are based on recently developed techniques to probe cellular microenvironments (*22*). More specifically, we focus on space- and time-resolved maps of pH levels obtained through the deployment of arrays of ratiometric fluorescent microsensors across a cell culture (*23*). In short, pH values measured over time at a large number of points across the culture can be used to infer—for each cell in the population—the net import or export flux of protons upon assuming that local pH levels (i) equilibrate faster than a few minutes (the temporal resolution of the experiments) and (ii) are only affected by intercellular exchanges of acids (e.g., lactate) and by the buffering activity of the medium. The specific case we analyze concerns the early adaptation (lag phase) of a mixed population of human pancreatic cancer cells and cancer-associated fibroblasts sharing the same carbon- and oxygen-rich medium, in which single-cell proton fluxes obtained via statistical inference could be linked directly to lactate uptakes and outtakes. For our modeling work, we reduced the setup to the bare essentials. The reader is referred to (*19*) for details of the empirical data on which we rely.

Our modeling frame is as follows. In an $L \times L$ square (corresponding to the observable frame, where $L \simeq 0.5$ mm and where we neglect the z direction that is present in experiments because cells adhere to the substrate), $N \simeq 150$ cells of radius $R \ll L$ ($R \simeq 10\,\mu$m) are placed at fixed positions $\mathbf{r}_i$ [in agreement with the highly reduced mobility seen empirically (*19*)]. For each cell, a flux variable $u_i(t)$ (in units of millimoles per gram of dry weight per hour: mmol/gh) is given, corresponding to the net import ($u_i > 0$) or export ($u_i < 0$) of a certain compound—lactate in our case—over a large (10-min) time window ending at time t. This compound translocates through the culture by ordinary diffusion [i.e., advection is negligible, see (*19*) and section S5]. The task is to reconstruct the intercellular exchange network at all time steps, i.e., find time-dependent exchange fluxes $u_{i\to j} > 0$ such that

$$\sum_{j:u_j>0} u_{i\to j} \leq -u_i \tag{1}$$

if $u_i < 0$ (i.e., if cell i is an exporter, where the difference between the two sides of the inequality stands for the net flux accumulating in the medium and/or leaving the frame), and

$$\sum_{j:u_j<0} u_{j\to i} = u_i \tag{2}$$

if $u_i > 0$ (cell i is an importer). Equivalently, we would like to compute the probability $P(j\,|\,i)$ that a molecule absorbed by a cell at position $\mathbf{r}_j$ was excreted by a cell at position $\mathbf{r}_i$, as intercellular exchange fluxes are asymptotically given by

$$u_{i\to j} = u_j P(j\,|\,i) \tag{3}$$

In principle, because of the assumed separation of timescales, the matrix $P(j\,|\,i)$ can be found by solving a system of interconnected exit problems, i.e., Laplace equations with complex boundary conditions defined by cells acting as sources or sinks, as well as by the system's boundary (*24*). Because diffusion is the only transport mechanism involved, however, one may expect that $P(j\,|\,i) \propto 1/d_{ij}$, where $d_{ij} = |\,\mathbf{r}_i - \mathbf{r}_j\,|$ is the distance between the cell at point i and that at point j. A simple pairwise approximation would indeed suggest

Downloaded from https://www.science.org at Politecnico Di Torino on September 03, 2025

$$u_{i\to j} \simeq -\frac{1}{Z_i}\frac{u_i u_j}{d_{ij}} \tag{4}$$

where $u_i < 0$ (i is exporting), $u_j > 0$ (j is importing), and

$$Z_i = \sum_{k:u_k>0} \frac{u_k}{d_{ik}} \tag{5}$$

is a normalization factor required for dimensional reasons. Strictly speaking, however, Eq. 4 neglects both screening effects (i.e., it holds for two isolated cells) and material losses and accumulation in the medium (i.e., it implies equality in Eq. 1). The exact solution has to be obtained numerically. One possibility is to resort to a Monte Carlo method that simulates the two-dimensional diffusion process ["walk on spheres," (*25*); see section S1]. For our extensive numerical analysis, we, however, devised a computationally less demanding alternative that, as we shall see, yields quantitatively comparable results.

Stochastic Voronoi approach and empirical networks

In short, to build a computationally efficient protocol, one would like to coarse-grain the physical processes underlying exchanges in a convenient way. Because diffusion is the key driver of exchanges, distances to absorbers are expected to play a central role. A natural way of partitioning space based on these quantities consists in tessellating it à la Voronoi.

We therefore begin by dividing the $L \times L$ square into Voronoi tiles starting from the positions of absorbing cells (*26*) (Fig. 1A). Now, focus on a specific absorbing cell (with $u_i > 0$) whose tile is formed by n segments of length ℓ_k ($k = 1, \ldots, n$). Following, e.g., (*27*), we can concentrate on the asymptotic probabilities of the fates of a random walk, corresponding to the diffusion of a molecule, in this tile. The probability p_b that the walk hits the outer boundary of the tile is asymptotically given by the ratio between the overall length of the outer boundary ($\sum_k \ell_k$) and the sum of the lengths of the outer ($\sum_k \ell_k$) and inner ($2\pi R$, with R the cell's radius) boundaries

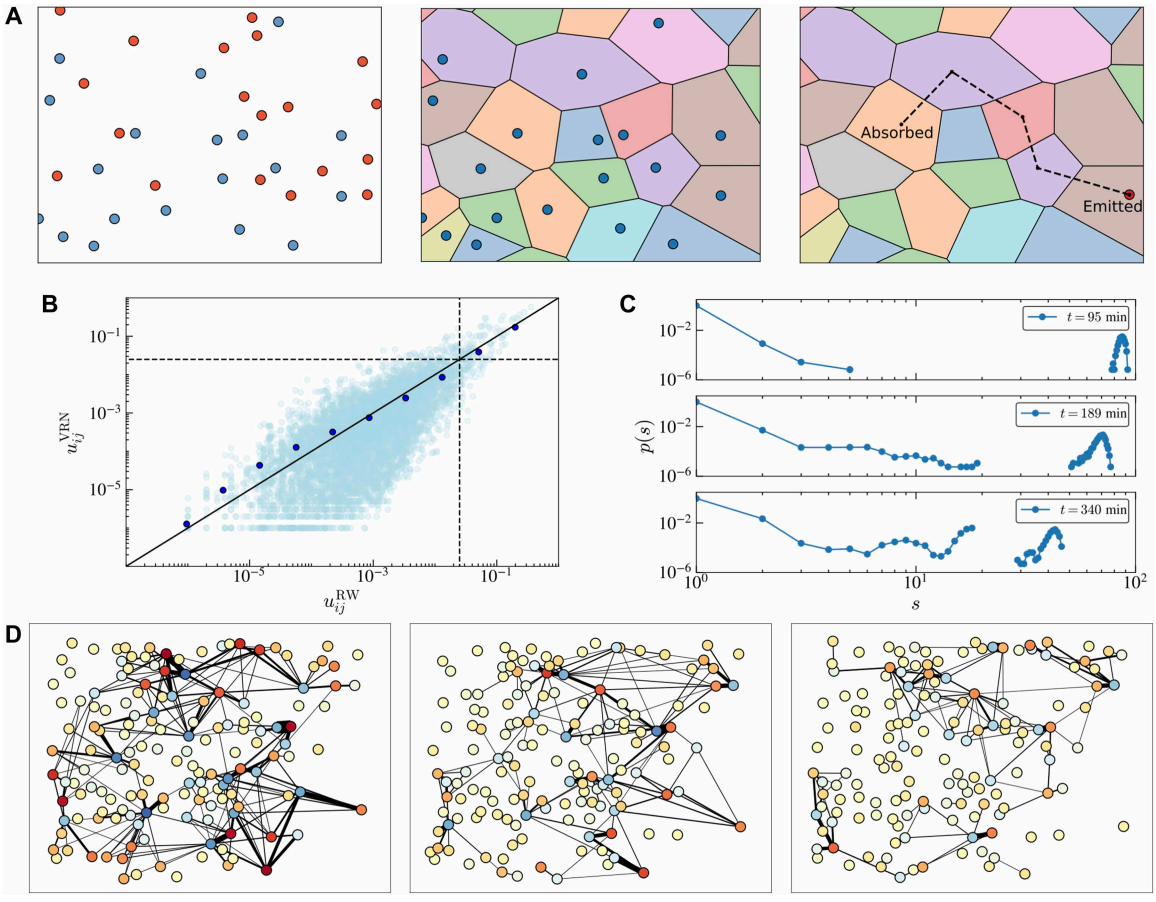

Fig. 1. Reconstruction of the empirical cross-feeding network during the Warburg effect. (**A**) Representative diagram showing a population of cells exchanging a compound in a shared environment. Each circle corresponds to a cell; red circles denote emitters; blue ones denote absorbers. Positions are derived from an actual experimental snapshot from (*19*). On the basis of these positions, we construct a Voronoi tessellation using absorbers as centers. The algorithm we use allows us to calculate the probability that a particle secreted by an emitter cell gets absorbed in any given tile. (**B**) Comparison between exchange fluxes (measured in millimoles per gram per hour, mmol/gh) obtained via the Voronoi-based method (vertical axis) and the (exact) Monte Carlo method described in section S1 (horizontal axis), for the first frame from the dataset given in (*19*). Dark markers represent averages computed upon binning data. The dashed lines mark the threshold $\theta = 0.025$ mmol/gh, such that cells with larger exchange fluxes are defined to be topologically connected. (**C**) Distribution of size (s) clusters of cells exchanging lactate, obtained from experimental data (*19*) ($N \simeq 150$ cells) at times $t = 95$, 189, and 340 min (top to bottom). (**D**) Reconstructed networks based on the mean single-cell lactate exchange fluxes corresponding to the time stamps shown in (C). Note how the largest cluster of exchanges that initially dominates the population gradually dissipates as the population partitions into smaller exchange clusters.

Downloaded from https://www.science.org at Politecnico Di Torino on September 03, 2025

$$p_b = \frac{\sum_k \ell_k}{2\pi R + \sum_k \ell_k} \tag{6}$$

On the other hand, the probability p_c that the molecule hits the center of the Voronoi tile (i.e., the absorbing cell) is just

$$p_c = 1 - p_b = \frac{2\pi R}{2\pi R + \sum_k \ell_k} \tag{7}$$

If, once it hits the cell, the molecule is absorbed with probability p_a, then the total probability p_{abs} that it is absorbed within that tile is obtained by summing the probabilities of all walks that end with an absorption event. Noting that the probability that a walk hits the cell n times without being absorbed is $p_c^n(1-p_a)^n$, we have

$$p_{abs} = p_c\ p_a \sum_{n\geq 0} p_c^n (1-p_a)^n = \frac{p_c\ p_a}{1-p_c(1-p_a)} \tag{8}$$

where the term $p_c p_a$ accounts for the probability that an absorption event follows n nonabsorption ones. As a consequence, the molecule escapes the tile by crossing one of its boundaries with probability $p_{esc} = 1 - p_{abs}$, and escape occurs through the kth boundary segment with probability

$$p(k\,|\,\mathrm{esc}) = \frac{\ell_k}{\sum_k \ell_k} \tag{9}$$

Assuming there are N_A absorbing cells, the complete random walk of a particle across the tiled square can therefore be seen as a Markov chain with $N_A + 1$ states (N_A states for "particle is in rth tile" with $r = 1, \ldots, N_A$ plus one state, labeled "0," corresponding to "absorbed") and transition probabilities given by

$$W(r \to s) = (1 - p_{abs,r}) \frac{\ell_{rs}}{L_r} \tag{10}$$

$$W(r \to 0) = p_{abs,r} \tag{11}$$

where $r, s \in \{1, \ldots, N_A\}$, $p_{abs,r}$ denotes the probability that the particle is absorbed in tile r, ℓ_{rs} is the length of the segment shared by tiles r and s (equal to zero if r and s are not neighbors), and L_r is the length of the outer boundary of tile r ($L_r = \sum_s \ell_{rs}$). This implies that $P(j\,|\,i)$, the probability that a particle emitted by cell i is absorbed by cell j, can be approximated numerically for all j and i by iterating the Markov chain just described a sufficiently large number of times using emitting cells as initial conditions for the random walks. Specifically

$$P(j\,|\,i) \simeq \frac{M(j\,|\,i)}{\sum_k M(j\,|\,k)} \tag{12}$$

where $M(j\,|\,i)$ is the number of molecules emitted at i that are absorbed at j. In summary, we derive $P(j\,|\,i)$ from Eq. 12 by iterating the Markov chain described by Eqs. 6 to 11, and subsequently compute $u_{i\to j}$ from Eq. 3. Note that $P(j\,|\,i)$ also depends on the cell radius R via Eqs. 6 and 8.

The main advantage of this approach lies in its low computational cost compared, e.g., to exact Monte Carlo methods: Once the Voronoi tessellation is found, relevant quantities can be calculated straightforwardly. Figure 1B shows that results obtained through the Voronoi method are in excellent agreement with those obtained from Monte Carlo when applied to a representative case [the first frame from the dataset in (*19*)].

Note how calculated exchange fluxes for empirical populations vary over roughly six orders of magnitude. Such a strong heterogeneity is a robust feature of empirical data. To focus the network structure on notable exchanges, however, we apply a threshold criterion on the value of $u_{i\to j}$: A connection between i and j will be assumed to be present only if $u_{i\to j}$ exceeds the minimum rate at which lactate accumulates in the medium as a result of the collective activity of all cells, which is found empirically to be roughly equal to $\theta = 0.025$ mmol/gh (*20*). Any exchange flux below θ would, in practice, be indistinguishable from this background. [Such a threshold also effectively matches the mean experimental error on single-cell lactate fluxes (*19*)].

The topologies of the resulting networks can be analyzed by different quantitative measures. The simplest possibility is to study the distribution of cluster sizes, whereby two cells are considered to be in the same cluster when they are either joined by an above-threshold exchange flux or by a chain of such fluxes, independently of their direction. A few representative distributions are shown in Fig. 1C. One sees that the exchange network derived from the experimental dataset is characterized by the rapid formation, and subsequent slow decay, of a large component of connected exchanges involving, at its maximum, up to 70% of cells. Such a behavior is observed robustly in all realizations of the reconstructed network, as roughly 40% of the individual links can be reconstructed accurately (see section S2). Snapshots displaying this scenario at three different times are shown in Fig. 1D. This dynamics can be compared to that of lactate spillover discussed in (*19*). Because lactate spillover decreases over time in experiments, densely networked states are characterized by larger lactate spillover in the medium compared to more fragmented states, in which exchanges are well balanced and spillover is reduced.

Because in the original dataset individual cells are labeled as being either tumor cells or fibroblasts, we can also appraise whether these types contribute differently to the exchange network, both topologically and over time. Specifically, starting from the pairwise exchanges, we can look for biases in the community-level exchange matrix between the tumoral and stromal components as a function of time, which amounts effectively to obtaining the bias matrix of a degree-corrected stochastic block model from the known solution of its inverse problem (community detection) (*28*). We found the bias matrix to be homogeneous within the error (see section S3): That is, the community structure is not detectable in intercellular exchanges. This is in line with previous results showing that acid flux distributions for tumor cells and fibroblasts are effectively identical (*19*).

The network reconstruction methods presented here exploit the fact that transport in our system is purely diffusive. One can, however, generalize them to the case in which an advective flow is also present. In practice, this requires a modulation of Eq. 9 that deforms the random walk in the direction of advection, so that the stronger the advection, the more aligned with it the walk. This extension is reported in section S4.

Constraint-based metabolic model

In view of the fact that the activities of a large number of cells contribute to the formation and dynamics of the exchange network, the above results raise two broad theoretical questions. First, can the dense-to-sparse crossover in exchanges we observe in experiments be explained in terms of a transition in the collective behavior of the

Downloaded from https://www.science.org at Politecnico Di Torino on September 03, 2025

system? This would directly indicate that, despite being spatially separated, cells do not make fully autonomous metabolic choices but, rather, use diffusing signals to coordinate their behavior, likely to achieve a better control of their microenvironments. Second, if so, how would such a coordination be connected with the metabolic activity of individual cells? To get some insight, it is necessary to view the empirical exchange network as an emergent feature of the activities of a large number of metabolic networks (the individual cells) that respond to local cues like nutrient and pH levels. To implement such a "network of networks" approach, we studied the exchange networks generated by a minimal model of a spatially organized population of N interacting metabolic networks, first introduced in (*20*).

The single-cell metabolic model is summarized in Fig. 2 (A and B). The metabolism of cell i is assumed to be fully described by three variables, namely, the glucose import flux $0 \le u_{G,i} \le U_G$, the oxygen import flux $0 \le u_{O,i} \le U_O$, and the flux of lactate exchange with the medium $u_{L,i}$, whereby $u_{L,i} > 0$ if cell i imports lactate and $u_{L,i} < 0$ if cell i exports lactate. The constants U_G and U_O stand for the finite capacity of cells to accommodate for glucose transporters and mitochondria, respectively. At steady state, the three fluxes are related by a condition expressing carbon mass balance. Considering the stoichiometry of glucose, lactate, and oxygen reported in Fig. 2A, one sees that $u_{G,i}$, $u_{L,i}$, and $u_{O,i}$ have to be related by

$$u_{G,i} + \frac{u_{L,i}}{2} = \frac{u_{O,i}}{6} \quad \forall i \tag{13}$$

which leaves two independent fluxes per cell. Moreover, each cell is bound by stoichiometry to produce energy [adenosine triphosphate (ATP)] at flux

$$u_{ATP,i} = 2u_{G,i} + \frac{14}{3}u_{O,i} \tag{14}$$

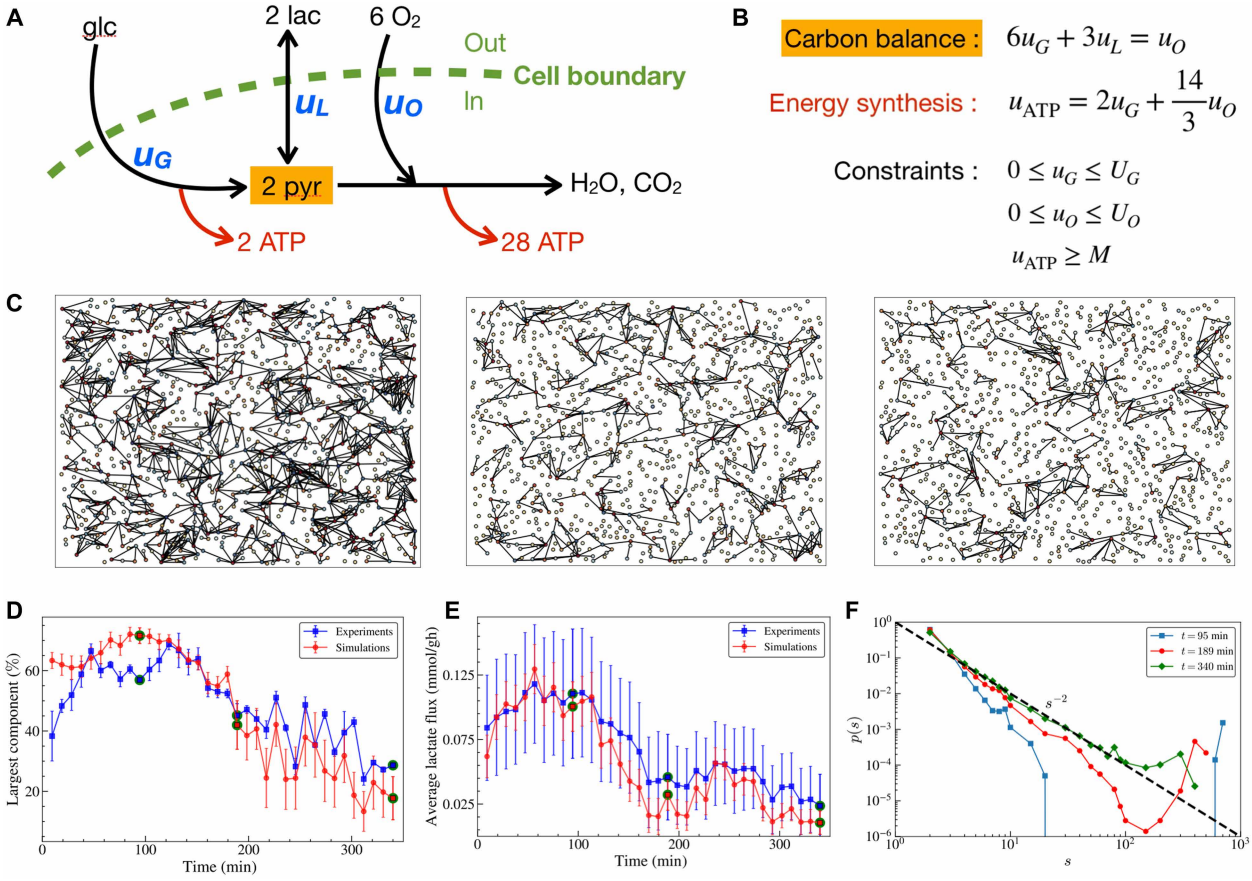

Fig. 2. A multicellular metabolic network model recapitulates experimental data. (**A**) Intracellular metabolic network model based on glucose (glc) and oxygen (O_2) import fluxes, and on lactate (lac) exchange with the medium. "pyr" represents pyruvate, the endpoint of the glycolysis pathway; "ATP" stands for adenosine triphosphate. The numerical coefficients represent the overall stoichiometry of the different pathways. (**B**) Stoichiometric equations describing carbon (pyr) mass balance and energy (ATP) synthesis, and bounds on import fluxes and energy synthesis, valid for each cell. In absence of competition for glucose and oxygen, all flux configurations of an N-cell system that are compatible with single-cell constraints and with the global constraint (*15*) induced by lactate exchanges are feasible. (**C**) Representative exchange networks reconstructed from simulations of a population of cells (each carrying a metabolic network whose state on average is inferred from experiments) globally coupled by diffusion. Parameter values are given in table S1; open boundary conditions are assumed. Results are shown for values of (β_O, β_G) corresponding to times $t = 95$ min ($\beta_O = -0.7, \beta_G = -1.45$), $t = 189$ min ($\beta_O = -1.4, \beta_G = -7.85$), and $t = 340$ min ($\beta_O = -1.9, \beta_G = -10.35$), as in Fig. 1D. (**D**) Average fraction of cells in the largest connected component found in experiments (blue) and computations (red) (average over 1000 network samples for each time frame). (**E**) Average lactate flux computed from Eq. 13 found in experiments (blue) and simulations (red) (average over 1000 network samples for each time frame). (**F**) Distribution of cluster sizes from simulations for the representative times used in (C) and in Fig. 1D. The black dashed line displays the power-law behavior $p(s) \sim s^{-2}$. This is to be compared with the empirical results shown in Fig. 1C.

Downloaded from https://www.science.org at Politecnico Di Torino on September 03, 2025

To sustain survival, it is required that $u_{\mathrm{ATP},i} \geq M$ for all i, with M being a value reflecting a minimum necessary (maintenance) rate of energy production. Values for the parameters U_{G}, U_{O}, and M can be taken from the literature (see table S1). Reaction fluxes of feasible single-cell metabolic states therefore satisfy the constraints shown in Fig. 2B. This is a widely used minimal version of more biochemically detailed constraint-based models of a metabolic network (*2*, *15*, *29*, *30*), which is known to capture many stylized features of more realistic schemes (*31*).

To model a population of N cells occupying a two-dimensional square, we assume that each cell i ($i = 1, \ldots, N$) has a preassigned position $\mathbf{r}_i$ in the square and carries a metabolic network as described above. When N such networks interact in a shared medium without competing for external nutrients (to comply with the nutrient abundance used in experiments), an effective coupling between cells can be induced by lactate exchanges. In absence of external sources of lactate, any spillover in the medium must indeed be endogenous, i.e., due solely to the activity of cells. This translates into a set of system-wide conditions on the lactate fluxes of different cells. Specifically, one finds that (*20*)

$$\sum_{j=1} A_{ij} u_{\mathrm{L},j} \leq 0 \quad \forall i \tag{15}$$

where (R being again the cell radius)

$$A_{ij} = \delta_{ij} + \left(1 - \delta_{ij}\right) \frac{R}{|\mathbf{r}_i - \mathbf{r}_j|} \tag{16}$$

are coefficients that account for the fact that lactate exchanges are diffusion limited. In these conditions, a feasible state of the N-cell system corresponds to a pair of fluxes $\left(u_{\mathrm{G},i}, u_{\mathrm{L},i}\right)$ per cell that satisfies the constraints given in Fig. 2B, plus the global constraint (Eq. 15).

To explore the space of feasible states, we weigh N-cell configurations according to the Boltzmann factor

$$e^{\beta_{\mathrm{G}} \sum_i u_{\mathrm{G},i} \; + \; \beta_{\mathrm{O}} \sum_i u_{\mathrm{O},i}} \tag{17}$$

where the auxiliary "inverse temperatures" β_{G} and β_{O} modulate the average flux state of the population, specifically the mean glucose (β_{G}) and oxygen (β_{O}) import fluxes. (We choose to represent states via the glucose and oxygen fluxes, which suffice to determine the missing lactate and energy fluxes for each cell.) The choice (Eq. 17) is tightly related to the maximum-entropy models of metabolism described in (*32*, *33*), which represent the least biased models compatible with experimental data on average fluxes. Here, however, it serves the main purpose of allowing for a compact representation of the metabolic state of the whole N-cell population using only the parameters β_{G} and β_{O}. In particular, their values can be fixed so as to reproduce the empirical statistics of lactate fluxes via a maximum likelihood approach through simulations of the system on a grid, as explained in (*20*). Because the statistics of lactate fluxes changes over time, the values of β_{G} and β_{O} providing the best fit are also time dependent.

Snapshots of the emergent exchange network found for a system with $N = 10^3$ cells are displayed in Fig. 2C. The time evolution found in empirical data is qualitatively reproduced, as the dense exchange network that initially spans across the population gets gradually diluted into smaller disconnected clusters. Such a trend is also clear from the behavior of the relative size (fraction of cells involved) of the largest exchange cluster (Fig. 2D) and from the population-averaged lactate flux (Fig. 2E), both of which quantitatively mimic the time trends retrieved from experimental data. Notice that, while the theoretical mean lactate flux ultimately yields a consistency check for the inference protocol, the relative size of the largest cluster is a genuine prediction of the model.

The behavior of the probability distribution of the sizes of clusters $p(s)$ is especially noteworthy (Fig. 2F). At earlier times, $p(s)$ is dominated by a single "giant" cluster. As time progresses, a large cluster persists (albeit reduced in size) along with a substantial number of smaller clusters. At later times, however, when the exchange network is fully fragmented, $p(s)$ is well described by a power-law decay with an exponent approximately equal to 2. Intriguingly, this value effectively matches the critical exponent characterizing the distribution of cluster sizes in two-dimensional percolation [$\simeq 187/91 = 2.0549 \ldots$ (*34*)].

To generalize the metabolic model to account for an advective flow of velocity v, one effectively has to replace the simple $1/r$ decay of the coupling matrix (Eq. 16) with an attenuation factor of the form $(1/r)\; e^{-v r(1-\cos\theta)/D}$, where θ is the angle between the vector distance of the two cells and the direction of the flow and D is the diffusion constant of the exchanged compound. In broad lines, advection hampers interactions and polarizes them in the direction of the flow, as described in detail in section S4.

Mean-field theory: Critical line for the emergence of an extensive exchange cluster

To rationalize these findings mathematically, let us focus on one cell and partition the space around it in circular stripes of width equal to the cell radius R. In this way, the surface area of the kth stripe equals $(2k+1)\pi R^2$. If cells are distributed homogeneously in space with density ρ, the number of cells in the kth stripe is a binomial random variable with average given by $\mu_k = (2k+1)\pi R^2 \rho$. For tractability, in the following, we approximate it with a Poisson random variable with the same average. If we now let x denote the probability that our cell belongs to the infinite percolating cluster (i.e., that it is connected to it by a nonzero exchange flux) and assume that the lactate fluxes of individual cells are independent and identically distributed random variables, we have

$$1 - x = \prod_{k \geq 1} \sum_{n \geq 0} e^{-\mu_k} \frac{\mu_k^n}{n!} \sum_{l=0}^{n} \binom{n}{l} (1-x)^l x^{n-l} P_k^{n-l} \tag{18}$$

where P_k stands for the probability that the cell is not exchanging lactate with a cell in the k-stripe. To see why Eq. 18 holds (i.e., why the right-hand side is the complement of x), note first that the term $(1-x)^l x^{n-l} P_k^{n-l}$ represents the probability that, if n cells inhabit the kth stripe from our cell, the latter is not connected to l of them and is exchanging lactate below the threshold with the remaining $n - l$ cells. By weighting each such factor with $\binom{n}{l}$ and summing over l, we are therefore computing the probability that the cell is effectively isolated from all of the n cells in the kth stripe. We next sum over n (which, as said above, is taken to be Poissonian) and lastly impose that this must hold for all stripes, i.e., take the product over k. Now, note that

$$\sum_{l=0}^{n} \binom{n}{l} (1-x)^l x^{n-l} P_k^{n-l} = \left(1 - x + x P_k\right)^n \tag{19}$$

and that

$$\sum_{n \geq 0} e^{-\mu_k} \frac{\mu_k^n}{n!} \left(1 - x + x P_k\right)^n = e^{-\mu_k} \; e^{\mu_k [1 - x(1 - P_k)]} \tag{20}$$

Downloaded from https://www.science.org at Politecnico Di Torino on September 03, 2025

which leads to

$$1-x=\prod_{k\geq 1}e^{-\mu_k x\left(1-P_k\right)} \tag{21}$$

This equation is equivalent to the standard mean-field percolation formula (*34*)

$$\sum_{k\geq 1}\mu_k\left(1-P_k\right)=-\frac{\log(1-x)}{x} \tag{22}$$

which implies the emergence of a giant cluster when the sum on the left-hand side exceeds 1.

To proceed, we consider a continuum approximation for the quantity $\sum_{k\geq 1}\mu_k\left(1-P_k\right)$. Denoting by $Q(r)$ the probability that two cells at distance r are connected (i.e., that they exchange lactate with a flux above the threshold θ) and by ρ the density of cells, we have

$$\sum_{k\geq 1}\mu_k\left(1-P_k\right)\simeq\rho\int_R^L Q(r)2\pi r dr \tag{23}$$

We can now approximate $Q(r)$ as the probability that both the (incoming) flux of the absorbing cell (u_{abs}) and the (outgoing) flux of the emitting cell (u_{emi}) at the boundary of the absorbing cell exceed the significance threshold, the latter being damped by the factors $e^{-r/\xi}$ and R/r that take into account dispersion (with a characteristic screening length scale ξ) and absorption, respectively. We furthermore assume that the distributions of lactate fluxes are Gaussian, with averages and variances given by the maximum-entropy metabolic network model described in the previous section. [This effectively amounts to neglecting the linear boundaries of the high-dimensional space of feasible flux vectors (*35*).] With this approximation, we get

$$Q(r)\simeq 2\ \Phi\left(|u_{\mathrm{abs}}|\geq\theta\right)\ \Phi\left(|u_{\mathrm{emi}}|\geq\theta e^{r/\xi}r/R\right) \tag{24}$$

where Φ denotes the cumulative Gaussian distribution function. The above expression can be inserted into Eq. 23 to retrieve the critical line from the condition $\log(1-x)/x=-1$ as a function of β_G and β_O, provided we have an expression for the screening length scale ξ. As a minimal assumption, we can posit that ξ is a linear function of the average lactate flux, namely

$$\xi=A+B\langle u_L\rangle \tag{25}$$

The best fit of simulation results is obtained for $A\simeq 3.3\times 10^{-2}$ and $B\simeq -1.3\times 10^{-4}$.

Key results from this mean-field percolation theory are showcased in Fig. 3. We first focus on the relative size of the largest component of the exchange networks, corresponding to x, Eq. 21 (Fig. 3A). One clearly sees that the mean-field model qualitatively recapitulates results obtained in simulations for two-dimensional systems, albeit with a sharp dense-to-sparse transition instead of a smooth crossover. We also show (Fig. 3B) the distribution of cluster sizes from simulations performed at fixed $\beta_O=1$ above (blue, $\beta_G=2$), at (red, $\beta_G=0$) and below (green, $\beta_G=-3$) the critical line for the percolation transition: While the giant cluster arises below the transition line, the algebraic decay with an exponent close to 2 is most clearly visible at criticality. Last, Fig. 3C shows the critical line, defined by the condition $\log(1-x)/x=-1$, in the (β_O,β_G) plane. Generally speaking, for any β_O, large enough values of β_G drive the system into a sparse networked phase, while the global exchange network is dense otherwise. The mean-field critical line qualitatively recapitulates the behavior of the relative size of the largest cluster as found in simulations, including a reentrance that is predicted by the mean-field model and found in simulations at large negative β_G (Fig. 3A). The transition observed in the exchange network is therefore well captured by a simple mean-field percolation scenario.

Comparison of cross-feeding percolation and metabolic overflow

We can now revisit overflow metabolism in the light of the percolation phase transition scenario derived above. In (*20*), again by combining mathematical modeling and statistical inference, it was shown that, for any β_G, the mean lactate output by cells (equivalent to the

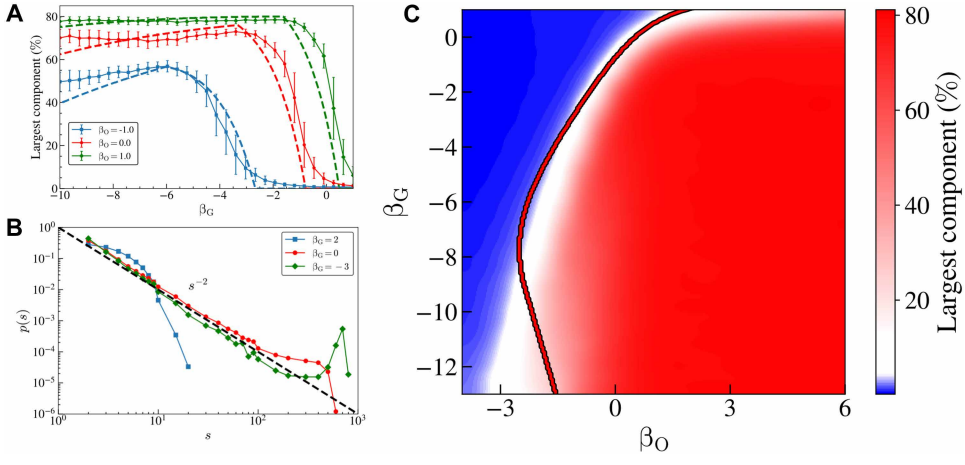

Fig. 3. Percolation cross-feeding transitions in the model. (**A**) Average size of the largest connected component (in terms of the fraction of nodes belonging to it) as a function of β_G, for different values of β_O. Results from simulations of a two-dimensional system are represented by the markers with errors (continuous lines being a guide for the eye), while analytical results from the mean-field theory are shown as dashed lines. Note that analytical results predict a sharp transition, as opposed to the crossover observed in simulations. (**B**) Distributions of cluster sizes for 3 different values of β_G and $\beta_O=1$. The dashed black line displays the power-law behavior $p(s)\sim s^{-2}$. (**C**) Critical line for the existence of an extensive cluster in the (β_O,β_G) plane as derived from mean-field theory. The background color map represents the relative size of the largest cluster from simulations of a two-dimensional system. Right of the critical line, the exchange network is system-spanning and dense; vice versa, left of the line, it is sparse and rich of small motifs. Again, the sharp transition predicted by mean-field theory turns into a smooth crossover in finite-dimensional simulations.

Downloaded from https://www.science.org at Politecnico Di Torino on September 03, 2025

lactate spillover in the medium) behaves markedly differently at high β_O compared to low β_O: In the former phase, no spillover in the medium (i.e., no acidification) occurs, while, in the latter phase, one is due to observe accumulation of lactate in the environment (Warburg effect). The line separating the two regimes in the (β_G, β_O) plane is shown in Fig. 4A, along with the line for the existence of a dense cluster and with the values of β_G and β_O describing the empirical population. Figure 4B displays instead the behavior of the relative size of the largest component and the lactate overflow flux along 3 vertical lines with constant β_O as a function of β_G.

One first notes that the mean-field approximation suggests the existence of four regions, depending on whether the exchange network is dense or sparse and on whether it is balanced (i.e., the lactate spillover is small) or not. While an overflow-sparse regime could have been expected based on the fact that aberrant cells should independently optimize their metabolism for growth (and hence lactate excretion), the system appears to evolve toward balanced states in an overflow-dense regime that is harder to explain within cell-autonomous models.

In addition, one can explicitly see how the reduction of lactate spillover is accompanied by the sparsification of the exchange network. By staying close to the critical overflow line, populations are likely to optimize the trade-off between the environmental costs of pollution (high in the overflow phase) and the regulatory costs of coordinating metabolisms (high in the balanced phase). The present results now suggest that different structures for exchange networks are associated to optimal trade-offs in different phases. In particular, contrary to early adaptation phases where system-scale exchange networks dominate, cellular behavior in balanced states appears to rely on multiple smaller communities of cells that keep microenvironmental acidification under control.

Note also how, in Fig. 4B, the lactate overflow transition occurs when the size of the largest percolation cluster is maximal as a function of β_G. Because, over time, the population (represented by the inferred values of β_G and β_O) tends toward states that maximize the energy yield on glucose (*20*), we can hypothesize that adaptation involves two intertwined processes. On shorter timescales, cells focus on the trade-off between environmental and regulatory costs, leading to dense exchange networks; on longer timescales, however, they aim at becoming more energy efficient individually, implying short-range coordination and reduced acid excretion (*2*). Both aspects are likely essential to formulate even a minimal dynamical model of how a population of cells adapts to an environment.

When advective transport coexists with diffusion (section S4), it reduces the ability of cells to exchange compounds, leading to more disconnected networks and increased lactate spillover in the medium. At the same time, though, lactate gets removed by the flow, so that environmental acid buildup is ultimately diminished.

DISCUSSION

The main result of this work is that, in a population of cells adapting to an environment, cells exchange lactate through a diffusion-mediated network whose topology varies in time as the adaptation proceeds. Here, we approached the problem of exchange network reconstruction quantitatively. In particular,

1) we devised a computationally efficient network reconstruction technique combining Voronoi tessellation of the culture with simple equilibrium results for absorption probabilities;

2) using this method, we showed that the experimental population undergoes a two-stage dynamics: Following inoculation, cells first build up a dense and intense exchange network comprising up to 70% of them; subsequently, as the adaptation proceeds, the network dilutes, eventually leading to the formation of smaller disconnected clusters of interacting cells;

3) we demonstrated that the key topological features of the inferred exchange networks (from the size of the largest component to the distribution of cluster sizes) are quantitatively reproduced by a minimal (maximum entropy–like) model that accounts for the metabolic behavior of cells and their interplay with the environment; the model is controlled by just two parameters, β_G and β_O, fixing on average mean glucose and oxygen consumptions of cells; and

4) by focusing on the general properties of the model, we showed that, as β_G and β_O change, exchange networks generically undergo a transition from a densely connected phase characterized by the presence of a large cluster of cells involved in mutual exchanges to a disconnected phase in which exchanges occur within small separated clusters. Such a transition can be studied quantitatively using methods of percolation theory, leading to a critical line in the (β_O, β_G) plane separating a dense exchange regime from a sparse

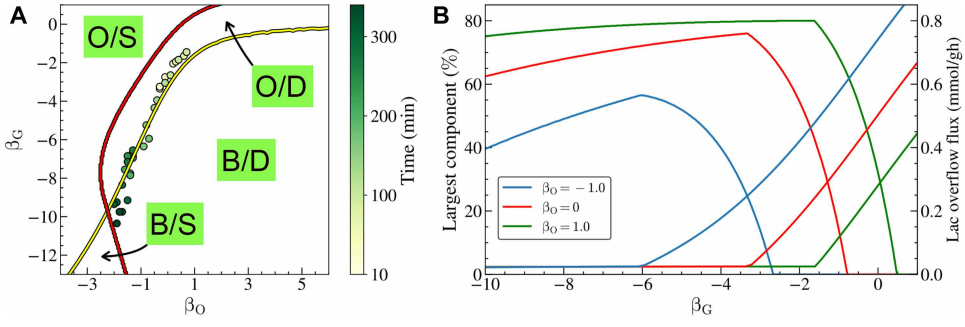

Fig. 4. Cross-feeding percolation and metabolic overflow. (**A**) Phase diagram of the multicellular metabolic network model in the (β_O, β_G) plane. Yellow line: overflow phase transition line dividing the plane into overflow (O) and balanced (B) phases, from (*20*). Red line: critical percolation line of lactate exchanges (from the mean-field approximation), dividing the plane into sparse (S) and dense (D) phases of the exchange web. Markers: values of β_O and β_G inferred from experimental data (color scale indicates the time step). The distinct regions correspond to overflow and sparse (O/S); overflow and dense (O/D); balanced and sparse (B/S); and balanced and dense (B/D). (**B**) Overflow curves (average lactate flux, right-side axis) versus percolation curves (relative size of the giant component from mean-field theory, left-side axis) as a function of β_G for three different values of β_O [i.e., along three vertical lines in the phase diagram of (A)].

Downloaded from https://www.science.org at Politecnico Di Torino on September 03, 2025

one. Real populations appear to evolve close to the crossover line as time progresses.

To rationalize these findings, we resorted to a time-independent modeling framework in which cells are only required to meet maintenance thresholds, exchanges are driven by diffusion, and changes in the ensuing intercellular network are modulated by the average level of carbon and oxygen intake by cells, measured respectively by the parameters β_G and β_O. We found that, for any given value of β_G, a dense network is expected for sufficiently large values of β_O. Conversely, the exchange network is sparse and dominated by small motifs for small enough β_O. Such a behavior can be associated to a percolation-like phase transition in the mean-field limit (see the phase diagram of Fig. 3C). Simulation results on a finite-dimensional system however effectively agree with this scenario. Therefore, as a population modulates its mean carbon and oxygen intakes over time, the network gradually adapts. Network inference results from empirical data show that the exchange matrix starts dense and becomes more and more sparse over time, approaching a state that resembles, at least statistically, a critical percolation network. No exogenous fine-tuning is required: Cells self-organize over time in response to changing microenvironmental conditions. In turn, the emergence of an exchange network effectively endows a population of cells with a substantial capability to control their environment by implementing a collective component in cellular metabolic strategies.

The critical percolation threshold for the exchange network formation and the phase transition line of the metabolic overflow do not coincide. This situation is similar to that found in studies attempting to derive a geometric interpretation for statistical observables in standard spin systems or in gas-liquid phase transition (*36*, *37*). In a nutshell, an equivalence between certain thermal ensemble-averaged quantities and percolative quantities is known to exist, upon a specific redefinition of the percolation model (*38*). This observation has, in turn, inspired further theoretical insights (*39*) as well as the development of cluster algorithms for sampling near criticality (*40*). While beyond the scope of the present work, an analogous redefinition of percolation in the context of interacting cell models could, in our view, be equally fruitful. An important insight that our reconstruction method could offer into the causes of the Warburg effect concerns its possible dependence on the topology of the exchange network beyond just connectivity, e.g., via the presence of a nontrivial community structure. An initial analysis of inverse modeling bias using a stochastic block model that explicitly considered cell types (tumoral versus stromal) however did not yield positive results: No significant exchange bias can be detected in community-level fluxes (section S3). Further work is, however, needed to fully elucidate this point.

The fact that diffusion is the main driver of intercellular exchanges in the system we consider has played an important role in the theory we developed. Besides being the most basic transport mechanism in the physical world, diffusion is central in living systems as well, vastly predating circulation-driven transport in evolutionary terms (*41*). It guides a huge variety of processes in bacteria (*42*) and in consortia of unicellular organisms (*43*); it promotes intercellular communication and organization in systems ranging from to the embryo (*44*–*47*) to fully developed multicellular organisms [see, e.g., intercellular communication within extracellular matrices (*48*)]; and it sustains intercellular cross-feeding and signaling in higher tissues, particularly the brain (*49*–*54*). The circulatory system itself is built via diffusive intercellular exchanges [see (*55*) for a review and (*56*) for the specific case of veins formation in the wing disc of flies]. Having a good grasp of the properties of diffusion-driven exchange networks is therefore essential to understand biological function at the supracellular level.

On the other hand, some of the features we observe do not persist if an advective flow competes with diffusion. To see this quantitatively, we have generalized our theoretical framework to include a global flow that affects the population by transporting molecules along a preferred direction (see section S4). In short, at the topological level, one finds—perhaps expectedly—that the networks get more and more polarized in the direction of the flow, while the size of the largest component decreases, upon increasing the intensity of advection relative to diffusion, quantified by the Peclet number (*57*). Most notably, though, the average lactate efflux from cells increases as the Peclet number increases, implying that, in more strongly advective environments, cells are less capable of balancing spillovers and must therefore rely entirely on the external flow to remediate acidification. It is, however, noteworthy that the qualitative properties of the emergent exchange network are expected to remain diffusion-like until the Peclet number gets close to 1. Experiments conducted in properly controlled conditions may of course be able to validate or disprove these predictions.

To conclude, we remark that theoretical approaches to exchange network reconstruction problems from input/output fluxes have a long history in network theory (*58*, *59*). In the most involved instances (e.g., the reconstruction of weighted exchange networks from single-node data), rather nontrivial statistical mechanics is involved (*60*). In the present case, however, the fact that diffusion is the basic exchange mechanism offers a strong proxy for the exchange probability, thereby allowing us to figure out simpler solution method(s). On the other hand, our work effectively addresses an instance of a multilayer network (*61*), in which a large-scale exchange network arises from the more or less coordinated activity of a large number of single-agent networks (the metabolic networks of individual cells). As the key role of cell-to-cell communication becomes more and more clear through experiments, the theoretical problem of linking them to intracellular networks increasingly acquires importance. The methods developed here, which are scalable to include more detailed metabolic network models, can provide a solid starting point for this analysis.

MATERIALS AND METHODS

Experimental data

Experimental parameters (e.g., typical cell radius, size of the culture, etc.), along with values for single-cell lactate fluxes and cell positions, were taken from (*19*). Single-cell fluxes and cell positions were used to calculate exchange fluxes; other parameters guided the calibration of computer simulations as described below.

Computational methods

The code implementing the Voronoi-based Markov chain method, presented in Results, to infer intercellular exchanges from the underlying acid export and import fluxes is available online (*62*). Details of the exact Monte Carlo method used in Fig. 1B are instead given in section S1. The generalization to the case of advective-diffusive systems requires a rescaling of the transition probabilities, which can be derived from the stationary solution of the advection-diffusion equation. These steps are described in detail in section S4.

The significance threshold θ for exchange fluxes was taken to coincide with the slowest rate at which lactate accumulates in the medium

Downloaded from https://www.science.org at Politecnico Di Torino on September 03, 2025

in experiments, with the idea that smaller exchange fluxes would not be distinguishable from this global background. The robustness of the reconstructed exchange networks has been estimated from standard error propagation starting from the errors on the single-cell fluxes derived in (*19*). Details are reported in section S2.

The feasible space of the metabolic model was sampled according to a probability density proportional to Eq. 17 using a hit-and-run Monte Carlo method (*63*). Parameters were chosen so as to reproduce the experimental setup as closely as possible, except for the maximum glucose and oxygen uptake rates, the ATP maintenance flux, and the diffusion constant of lactate, which were taken from the literature (see table S1). This allowed us to use the same significance threshold θ used for the empirical network reconstruction. Last, the analysis of community-level exchanges was based on the stochastic block model (*28*) and is described in detail in section S3.

Supplementary Materials

This PDF file includes:

Supplementary Text
Figs. S1 to S5
Tables S1 and S2

REFERENCES AND NOTES

1. P. Ball, "How life works: A user's guide to the new biology," in *How Life Works* (University of Chicago Press, 2023).
2. B. Palsson, *Systems Biology* (Cambridge Univ. Press, 2015).
3. E. Klipp, W. Liebermeister, C. Wierling, A. Kowald, *Systems Biology: A Textbook*. (John Wiley & Sons, 2016).
4. U. Alon, *An Introduction to Systems Biology: Design Principles of Biological Circuits* (Chapman and Hall/CRC, 2019).
5. L. E. Reichl, *A Modern Course in Statistical Physics* (John Wiley & Sons, 2016).
6. L. Leuzzi, T. M. Nieuwenhuizen, *Thermodynamics of the Glassy State*. (CRC Press, 2007).
7. D. J. Amit, *Modeling Brain Function: The World of Attractor Neural Networks* (Cambridge Univ. Press, 1989).
8. W. Bialek, *Biophysics: Searching for Principles* (Princeton Univ. Press, 2012).
9. A. Vazquez, *Overflow Metabolism: From Yeast to Marathon Runners* (Academic Press, 2017).
10. M. Basan, S. Hui, H. Okano, Z. Zhang, Y. Shen, J. R. Williamson, T. Hwa, Overflow metabolism in *Escherichia coli* results from efficient proteome allocation. *Nature* **528**, 99–104 (2015).
11. M. Mori, T. Hwa, O. C. Martin, A. De Martino, E. Marinari, Constrained allocation flux balance analysis. *PLoS Comput. Biol.* **12**, e1004913 (2016).
12. M. Mori, E. Marinari, A. De Martino, A yield-cost tradeoff governs *Escherichia coli*'s decision between fermentation and respiration in carbon-limited growth. *npj Syst. Biol. Appl.* **5**, 16 (2019).
13. D. H. De Groot, J. Lischke, R. Muolo, R. Planqué, F. J. Bruggeman, B. Teusink, The common message of constraint-based optimization approaches: Overflow metabolism is caused by two growth-limiting constraints. *Cell. Mol. Life Sci.* **77**, 441–453 (2020).
14. M. G. Vander Heiden, L. C. Cantley, C. B. Thompson, Understanding the Warburg effect: The metabolic requirements of cell proliferation. *Science* **324**, 1029–1033 (2009).
15. A. Vazquez, J. Liu, Y. Zhou, Z. N. Oltvai, Catabolic efficiency of aerobic glycolysis: The Warburg effect revisited. *BMC Syst. Biol.* **4**, 58 (2010).
16. S. Schuster, D. Boley, P. Möller, H. Stark, C. Kaleta, Mathematical models for explaining the warburg effect: A review focussed on ATP and biomass production. *Biochem. Soc. Trans.* **43**, 1187–1194 (2015).
17. R. J. De Berardinis, N. S. Chandel, We need to talk about the Warburg effect. *Nat. Metab.* **2**, 127–129 (2020).
18. G. A. Brooks, The science and translation of lactate shuttle theory. *Cell Metab.* **27**, 757–785 (2018).
19. V. Onesto, S. Forciniti, F. Alemanno, K. Narayanankutty, A. Chandra, S. Prasad, A. Azzariti, G. Gigli, A. Barra, A. De Martino, D. De Martino, L. L. Del Mercato, Probing single-cell fermentation fluxes and exchange networks via pH-sensing hybrid nanofibers. *ACS Nano* **17**, 3313–3323 (2023).
20. K. Narayanankutty, J. A. Pereiro-Morejon, A. Ferrero-Fernández, V. Onesto, S. Forciniti, L. L. del Mercato, R. Mulet, A. De Martino, D. S. Tourigny, D. De Martino, Metabolic coordination and phase transitions in spatially distributed multi-cellular systems. *Commun. Phys.* **8**, 1–12 (2025).
21. N. Musat, F. Musat, P. K. Weber, J. Pett-Ridge, Tracking microbial interactions with nanosims. *Curr. Opin. Biotechnol.* **41**, 114–121 (2016).
22. G. Grasso, F. Colella, S. Forciniti, V. Onesto, H. Iuele, A. C. Siciliano, F. Carnevali, A. Chandra, G. Gigli, L. L. Del Mercato, Fluorescent nano-and microparticles for sensing cellular microenvironment: Past, present and future applications. *Nanoscale Adv.* **5**, 4311–4336 (2023).
23. R. Rizzo, V. Onesto, S. Forciniti, A. Chandra, S. Prasad, H. Iuele, F. Colella, G. Gigli, L. L. Del Mercato, A pH-sensor scaffold for mapping spatiotemporal gradients in three-dimensional in vitro tumour models. *Biosens. Bioelectron.* **212**, 114401 (2022).
24. D. Medková, "The Laplace equation," in *Boundary Value Problems on Bounded and Unbounded Lipschitz Domains* (Springer, 2018).
25. M. E. Muller, Some continuous monte carlo methods for the dirichlet problem. *Ann. Math. Stat.* **27**, 569–589 (1956).
26. F. Aurenhammer, R. Klein, "Voronoi diagrams," in *Computational Geometry* (Springer, 2000).
27. H. C. Berg, *Random Walks in Biology* (Princeton Univ. Press, 1993).
28. B. Karrer, M. E. J. Newman, Stochastic blockmodels and community structure in networks. *Phys. Rev. E* **83**, 016107 (2011).
29. R. A. Majewski, M. M. Domach, Simple constrained-optimization view of acetate overflow in e. coli. *Biotechnol. Bioeng.* **35**, 732–738 (1990).
30. J. Fernandez-de Cossio-Diaz, A. De Martino, R. Mulet, Microenvironmental cooperation promotes early spread and bistability of a Warburg-like phenotype. *Sci. Rep.* **7**, 3103 (2017).
31. F. Capuani, D. De Martino, E. Marinari, A. De Martino, Quantitative constraint-based computational model of tumor-to-stroma coupling via lactate shuttle. *Sci. Rep.* **5**, 11880 (2015).
32. D. De Martino, F. Capuani, A. De Martino, Growth against entropy in bacterial metabolism: The phenotypic trade-off behind empirical growth rate distributions in *E. coli*. *Phys. Biol.* **13**, 036005 (2016).
33. D. De Martino, A. M. Andersson, T. Bergmiller, C. C. Guet, G. Tkačik, Statistical mechanics for metabolic networks during steady state growth. *Nat. Commun.* **9**, 2988 (2018).
34. D. Stauffer, A. Aharony, *Introduction to Percolation Theory* (Taylor & Francis, 2018).
35. A. Braunstein, A. P. Muntoni, A. Pagnani, An analytic approximation of the feasible space of metabolic networks. *Nat. Commun.* **8**, 14915 (2017).
36. J. Kertész, Existence of weak singularities when going around the liquid-gas critical point. *Phys. A: Stat. Mech. Appl.* **161**, 58–62 (1989).
37. C. P. Schioppa, F. Sciortino, P. Tartaglia, Coniglio-Klein mapping in the metastable region. *Phys. Rev. E* **57**, 3797 (1998).
38. A. Coniglio, W. Klein, Clusters and ising critical droplets: A renormalisation group approach. *J. Phys. A Math. Gen.* **13**, 2775 (1980).
39. S. Fortunato, Critical droplets and phase transitions in two dimensions. *Phys. Rev. B* **67**, 014102 (2003).
40. R. H. Swendsen, J.-S. Wang, Nonuniversal critical dynamics in Monte Carlo simulations. *Phys. Rev. Lett.* **58**, 86–88 (1987).
41. N. H. Barton, D. Briggs, J. Eisen, D. Goldstein, N. Patel, *Evolution* (Cold Spring Harbor Laboratory Press, 2007).
42. A. L. Koch, "Diffusion: The crucial process in many aspects of the biology of bacteria," in *Advances in Microbial Ecology*, vol. 11, K.C. Marshall, Eds. (Springer, 1990).
43. F. J. Peaudecerf, F. Bunbury, V. Bhardwaj, M. A. Bees, A. G. Smith, R. E. Goldstein, O. A. Croze, Microbial mutualism at a distance: The role of geometry in diffusive exchanges. *Phys. Rev. E* **97**, 022411 (2018).
44. A. A. Teleman, S. M. Cohen, Dpp gradient formation in the drosophila wing imaginal disc. *Cell* **103**, 971–980 (2000).
45. A. D. Lander, Q. Nie, F. Y. M. Wan, Do morphogen gradients arise by diffusion? *Dev. Cell* **2**, 785–796 (2002).
46. O. Wartlick, P. Mumcu, A. Kicheva, T. Bittig, C. Seum, F. Jülicher, M. Gonzalez-Gaitan, Dynamics of dpp signaling and proliferation control. *Science* **331**, 1154–1159 (2011).
47. S. Matsuda, M. Affolter, Dpp from the anterior stripe of cells is crucial for the growth of the *Drosophila* wing disc. *eLife* **6**, e22319 (2017).
48. M. A. Swartz, M. E. Fleury, Interstitial flow and its effects in soft tissues. *Annu. Rev. Biomed. Eng.* **9**, 229–256 (2007).
49. M. Tsacopoulos, P. J. Magistretti, Metabolic coupling between glia and neurons. *J. Neurosci.* **16**, 877–885 (1996).
50. C. Nicholson, Diffusion and related transportmechanisms in brain tissue. *Rep. Prog. Phys.* **64**, 815 (2001).
51. E. Syková, C. Nicholson, Diffusion in brain extracellular space. *Physiol. Rev.* **88**, 1277–1340 (2008).
52. P. J. Magistretti, I. Allaman, Lactate in the brain: From metabolic end-product to signalling molecule. *Nat. Rev. Neurosci.* **19**, 235–249 (2018).
53. P. Gimenez Minguez, "The role of the brain extracellular space in diffusion and cell signalling," thesis, University of the Basque Country (UPV/EHU) (2023).
54. J. Tønnesen, S. Hrabtová, F. N. Soria, Local diffusion in the extracellular space of the brain. *Neurobiol. Dis.* **177**, 105981 (2023).

Downloaded from https://www.science.org at Politecnico Di Torino on September 03, 2025

55. D. Ambrosi, F. Bussolino, L. Preziosi, A review of vasculogenesis models. *Comput. Math. Methods Med.* **6**, 1–19 (2005).
56. P. S. Bosch, R. Ziukaite, C. Alexandre, K. Basler, J.-P. Vincent, Dpp controls growth and patterning in *Drosophila* wing precursors through distinct modes of action. *eLife* **6**, e22546 (2017).
57. R. Byron Bird, W. E. Stewai, E. N. Lightfoot, *Transport Phenomena* (John Wiley & Sons, 2002).
58. T. Squartini, D. Garlaschelli, *Maximum-Entropy Networks: Pattern Detection, Network Reconstruction and Graph Combinatorics* (Springer, 2017).
59. T. Squartini, G. Caldarelli, G. Cimini, A. Gabrielli, D. Garlaschelli, Reconstruction methods for networks: The case of economic and financial systems. *Phys. Rep.* **757**, 1–47 (2018).
60. R. Mastrandrea, T. Squartini, G. Fagiolo, D. Garlaschelli, Enhanced reconstruction of weighted networks from strengths and degrees. *New J. Phys.* **16**, 043022 (2014).
61. G. Bianconi, *Multilayer Networks: Structure and Function* (Oxford Univ. Press, 2018).
62. L. C. F. Latoski, llatoski/crossfeeding-percolation; https://zenodo.org/records/16741366.
63. D. De Martino, M. Mori, V. Parisi, Uniform sampling of steady states in metabolic networks: Heterogeneous scales and rounding. *PLOS ONE* **10**, e0122670 (2015).

Acknowledgments

Funding: L.C.F.L. acknowledges partial funding from Conselho Nacional de Desenvolvimento Científico e Tecnológico (CNPq). A.D.M. is supported by the European REA, Marie Skłodowska-Curie Actions, grant agreement no. 101131463 (SIMBAD). D.D.M. acknowledges financial support from grants PIBA_2024_1_0016 (Basque Government) and Project PID2023-146408NB-I00 funded by MICIU/AEI/10.13039/501100011033 and by FEDER, UE. **Author contributions:** Conceptualization, supervision, writing, and funding: A.D.M. and D.D.M. Modeling, methodology, analysis, and validation: L.C.F.L., A.D.M., and D.D.M. Simulations: L.C.F.L. and D.D.M. Figures: L.C.F.L. **Competing interests:** The authors declare that they have no competing interests. **Data and materials availability:** All data needed to evaluate the conclusions in the paper are present in the paper and/or the Supplementary Materials. Codes are available in (*62*).

Submitted 8 January 2025
Accepted 6 August 2025
Published 3 September 2025
10.1126/sciadv.adv8216

Downloaded from https://www.science.org at Politecnico Di Torino on September 03, 2025